Growth Rates of the Ablative Rayleigh–Taylor Instability in Inertial Confinement Fusion

In recent years, several authors[1–14] have studied the linear growth of the Rayleigh–Taylor (RT) instability in ablation fronts accelerated by laser irradiations. The determination of the instability growth rate is crucial to the success of inertial confinement fusion (ICF)[15,16] because an excessive distortion of the front could lead to a severe degradation of the capsule performance with respect to the final core conditions by seeding the deceleration-phase RT instability and preventing the onset of the ignition process.

For a successful implosion, ICF targets must be designed to keep the RT growth at an acceptable level. Because of the complexity of 2-D or 3-D codes and the mesh refinement needed to simulate hydro-instabilities, 2-D or 3-D simulations cannot be routinely used to study the capsule stability and mixing. The best approach to target design is to carry out a preliminary analysis by using 1-D simulations to study the main characteristics of the implosion and then processing the data with a mixing model to study the evolution of the instability and the induced rms deviations. Once the preliminary design is completed, the optimization can be carried out by using 2-D or 3-D codes. Since the mixing model predictions are based on the initial perturbation amplitude and linear growth rates, it is very important to generate an accurate and reliable growth-rate formula to be used in conjunction with the 1-D code output.

According to the linear classical theory,[17] the interface between a heavy fluid of constant density ρ_h and a light fluid of constant density ρ_l in a gravitational field g pointing toward the light fluid is unstable. A small perturbation would grow exponentially in time, $\sim e^{\gamma_{\rm cl} t}$, at a rate

$$\gamma_{\rm cl} = \sqrt{A_T^{\rm cl}\, kg}\,, \tag{1}$$

where $A_T^{\rm cl} = (\rho_h - \rho_l)/(\rho_h + \rho_l)$ is the Atwood number and k is the perturbation wave number.

If the density is smoothly varying between the two fluids and the minimum density-gradient scale length $L_m = \min\left|\rho/(d\rho/dx)\right|$ is finite, then a distinction must be made between those modes with wavelength larger and smaller than L_m. The long-wavelength modes ($kL_m << 1$) are not affected by the finite L_m and grow according to Eq. (1), while the short-wavelength modes ($kL_m >> 1$) are localized inside the smooth interface and grow at the rate[18]

$$\gamma = \sqrt{\frac{g}{L_m}}\,. \tag{2}$$

An asymptotic formula reproducing the results at short and long wavelengths can be easily generated by inspection of Eqs. (1) and (2) leading to

$$\gamma = \sqrt{\frac{A_T^{\rm cl} kg}{1 + A_T^{\rm cl} kL_m}}\,. \tag{3}$$

In laser-accelerated targets, the ablation process and the thermal transport add a great deal of complication to the evolution of the instability. The overdense target material (with density ρ_a) is ablated at a rate $\dot{m} = \rho_a V_a$, where V_a is the ablation velocity. The latter represents the penetration speed of the ablation front in the overdense target. The ablated material blowing off the target rapidly expands inside the ablation front and accelerates to large velocities relative to the overdense targets.

Several authors[1–14] have shown that the ablation process leads to a reduction of the instability growth rate. The so-called ablative stabilization was first discussed in Ref. 1 and thereafter extensively studied in Refs. 2–13. Because of the mathematical complexity of the problem, simplified analytic models such as the sharp boundary model have been used to describe the linear phase of the instability. However, such models are

heuristic in nature as they lack a proper closure, which is left to the physical intuition. For such reasons, different authors using different closure equations have produced different growth-rate formulas (see Refs. 1, 5, and 12). Numerical simulations have confirmed the stabilizing effect of ablation and indicated that, in some cases (as described later), the growth rate can be approximated by the following formula:

$$\gamma = 0.9\sqrt{kg} - 3.1\, kV_a\,. \tag{4}$$

Equation (4) was derived in Ref. 3 by fitting the numerical solution of the linearized conservation equations including ablation and electronic heat conduction. As stated in the **Growth Rates** section, Eq. (4) does not correctly reproduce the growth rates in the presence of a significant radiation energy transport leading to smooth density profiles. It is important to observe that Eq. (4) does not include the stabilizing effect of finite density-gradient scale length and it can only be applied to very sharp ablation fronts or modes with $kL_m << 1$.

Only very recently, the analytic stability theory of accelerated ablation fronts has been carried out in the limit of subsonic ablation flows[8–12] (i.e., fronts with ablation velocity less than the sound speed at the ablation front) by using complicated asymptotic matching techniques. Subsonic ablation fronts are characterized by two dimensionless parameters:[10] the Froude number $Fr = V_a^2/gL_0$ and the power index for thermal conduction $\nu\left(\kappa \sim T^{\nu}\right)$. Here, L_0 is the characteristic thickness of the ablation front, which is proportional to the minimum value of the density-gradient scale length[6] $L_m\left[L_0 = L_m\nu^{\nu}/(\nu+1)^{\nu+1}\right]$. The analytic theory developed in Refs. 8–11 shows that the instability growth rate is strongly dependent on the magnitude of the Froude number. For large Froude numbers,[9,10] the main stabilizing effects are ablation and blowoff convection, and the growth rate can be written in the following form:[9,12]

$$\gamma = \sqrt{A_T kg - A_T^2\, k^2\, V_a\, V_{\text{b.o.}}} - \left(1 + A_T\right) kV_a\,, \tag{5}$$

where

$$A_T \equiv \frac{1-\left(\rho_{\text{b.o.}}/\rho_a\right)}{1+\left(\rho_{\text{b.o.}}/\rho_a\right)}, \qquad V_{\text{b.o.}} = V_a\,\frac{\rho_a}{\rho_{\text{b.o.}}}, \tag{6a}$$

$$\frac{\rho_{\text{b.o.}}}{\rho_a} = \mu_0\left(kL_0\right)^{1/\nu}, \qquad \mu_0 = \frac{(2/\nu)^{1/\nu}}{\Gamma(1+1/\nu)} + \frac{0.12}{\nu^2}, \tag{6b}$$

$\Gamma(x)$ is the gamma function and $V_{\text{b.o.}}$ is the velocity of the blowoff material at the distance $\sim\lambda$ from the ablation front. Observe that the cutoff wave number obtained by setting $\gamma = 0$ in Eq. (5) occurs at long wavelengths,[8]

$$k_c L_0 = \left[\frac{\mu_0(\nu)}{Fr}\right]^{\nu/(\nu-1)} \left\{1 + O\left[\left(kL_0\right)^{1/\nu}\right]\right\} << 1\,, \tag{7}$$

and short-wavelength modes are stable. As shown in Refs. 9 and 10, Eq. (5) can be accurately fitted by Eq. (4) for $\nu = 2.5$ and $0.1 < Fr < 5$, thus suggesting that the latter can be applied to ablation fronts with large Froude numbers.

When the Froude number is less than unity ($Fr << 1$), the analytic stability theory becomes more complicated and can be carried out only in the limits of $\in = kL_0 << 1$ and $\in >> 1$. The analysis of Ref. 11 has shown that long-wavelength modes with wave numbers $\in << 1$ have a growth rate $\gamma \simeq \sqrt{A_T kg} - \beta kV_a$, where $1 < \beta < 2$ is a function of ν, $\beta = \Gamma\left(1+2/\nu\right)/\Gamma^2\left(1+1/\nu\right)$. Short-wavelength modes ($kL_0 > 1$) are unstable, and the corresponding perturbations are mitigated by ablative convection, finite density gradient, and thermal smoothing. Their growth rate can be written as

$$\gamma = \sqrt{\alpha g/L_0 + c_0^2 k^4 L_0^2 V_a^2} - c_0 k^2 L_0 V_a$$

for $1 << kL_0 << Fr^{-1/3}$, and

$$\gamma = c_1 g/\left(V_a k^2 L_0^2\right) - c_2 kV_a$$

for the wave numbers near the cutoff ($k \approx k_c$). The parameters α and c_{0-2} have lengthy expressions described in Ref. 11, and a complete summary of the growth-rate formulas is given in Table 1 of Ref. 11. The cutoff wave number k_c of ablation fronts with small Froude numbers occurs at short wavelengths and scales as $k_c L_0 \sim Fr^{-1/3} >> 1$.

The growth-rate formulas obtained in Ref. 11 for small Froude numbers and short/long wavelengths can be combined with the formula (5) for large Froude numbers into a single expression that reproduces the analytic results in the appropriate limits ($Fr << 1$, $Fr >> 1$, $\in << 1$, $\in >> 1$). According to

Ref. 11, the asymptotic formula can be written in the following form:

$$\gamma = \sqrt{\hat{A}_T kg + \delta^2 k^4 L_0^2 V_a^2 + \left(\omega^2 - \frac{1}{\xi_l}\right) k^2 V_a^2} - \delta k^2 L_0 V_a - \hat{\beta} k V_a , \tag{8a}$$

where

$$\hat{A}_T = \frac{\xi_h - \xi_l}{\xi_h + \xi_l}, \qquad \xi_h = \left(1 + K_1 e^{-\frac{K_3}{\epsilon}}\right)^{-1},$$
$$\xi_l = \mu_0 \left(\frac{1}{\epsilon} + K_2\right)^{-\frac{1}{\nu}}, \tag{8b}$$

$$\hat{\beta} = \omega \frac{1 + T_1 \epsilon}{1 + T_2 \epsilon}, \quad T_1 = \frac{\beta_0 - \beta_1}{\beta_2 \beta_0},$$
$$T_2 = \frac{\beta_0 - \beta_1}{\beta_2 \beta_1}, \tag{8c}$$

$$\omega = \beta_0 \frac{1 + \left(1 + \hat{A}_T\right) \big/ \beta_0 \sinh(Fr)}{1 + \sinh(Fr)},$$
$$\beta_0 = \frac{\Gamma\left(1 + \frac{2}{\nu + 0.1/\nu^4}\right)}{\Gamma^2\left(1 + \frac{1}{\nu + 0.1/\nu^4}\right)}, \tag{8d}$$

$$\beta_1 = \frac{1}{\xi_0 \sqrt{5}}, \qquad \beta_2 = B + \frac{\beta_0^2 + \beta_1^2}{2\delta\beta_1} - \frac{1 + K_1}{2\delta\beta_1}, \tag{8e}$$

$$\delta = \frac{1}{2\Upsilon}\left[K_1 A + \frac{1}{\nu K_2} \times \sqrt{\left(\frac{1}{\nu K_2} + K_1 A\right)^2 - 4K_1\beta_1\Upsilon - \frac{1 + K_1 \nu}{\nu^2 K_2^2}}\right], \tag{8f}$$

$$\Upsilon = \frac{25}{8}\frac{\xi_0^{2\nu+1}}{2\nu + 3}, \quad K_2 = \left[(1 + K_1)\mu_0\right]^{\nu}, \quad K_1 = \frac{1}{\xi_0} - 1, \tag{8g}$$

$$K_3 = \frac{1 + K_1}{K_1}\left(2\delta\Upsilon - \frac{1}{\nu K_2}\right), \qquad \mu_0 = \frac{(2/\nu)^{1/\nu}}{\Gamma\left(1 + \frac{1}{\nu}\right)} + \frac{0.12}{\nu^2}, \tag{8h}$$

$$\xi_0 = \frac{2\nu + 2}{2\nu + 3},$$

$$A = \frac{\sqrt{5}}{4}\frac{\xi_0^{\nu-1}}{(2\nu + 3)^2} \times \left[\sqrt{\frac{2}{5}\xi_0}\left(12\nu^2 + 25\nu + 18\right) + \frac{\nu + 2}{2\nu + 3}\left(8\nu^2 + 20\nu + 17\right)\right], \tag{8i}$$

$$B = \frac{\sqrt{5}}{4}\frac{\xi_0^{\nu-1}}{(2\nu + 3)^2} \times \left[\sqrt{\frac{2}{5}\xi_0}\left(8\nu^2 + 25\nu + 12\right) - \frac{8\nu^3 + 16\nu^2 + 7\nu + 4}{2\nu + 3}\right]. \tag{8j}$$

A detailed comparison of the growth rates obtained by using Eq. (8) and the numerical solutions of the conservation equations has demonstrated a remarkable agreement over a wide range of values for Fr, ν, and ϵ (see Ref. 11).

Despite its lengthy expression, the asymptotic formula can be easily computed once the Froude number Fr, the length L_0, the acceleration g, the ablation velocity V_a, and the power index for thermal conduction ν are known. The main difficulty in using Eq. (8) lies in the determination of the equilibrium parameters whose values are strongly dependent on the dominant energy transport mechanism. In this article, we describe a simple procedure to be used in conjunction with existing one-dimensional hydrodynamic codes to determine Fr, L_0, g, V_a,

and ν. In addition, we apply this procedure to accelerated flat foils commonly used in ICF experiments and determine the unstable spectrum using Eq. (8). We also compare the analytic growth rates with the results of two-dimensional simulations obtained using the code *ORCHID*.[19] Numerical fits of Eq. (8) are also studied for different ablators, and simplified formulas are generated for a fast growth-rate estimate. It is the aim of this article to simplify the theoretical result of Betti *et al*. (Refs. 8–11) to make it useful to ICF target design.

Equilibrium Parameters

One-dimensional simulations are commonly used in ICF target design, and several 1-D codes describing laser-accelerated targets are available at universities and national laboratories. Among them, the most frequently used are the codes *LILAC*,[20] *HYADES*,[21] *LASNEX*,[22] etc. In this article, the authors have extensively used the code *LILAC*, a 1-D Lagrangian code including laser absorption, classical flux-limited thermal transport, and multigroup radiation diffusive transport. The equation-of-state package available in *LILAC* includes the ideal gas, Thomas–Fermi, and SESAME tables.

The analytic stability analyses are usually based on a single-temperature (or one-group) diffusive model for the heat transport, i.e., the heat flux is proportional to the temperature gradient, and the thermal conductivity follows a power law of the temperature, $\kappa = \kappa_a \left(T/T_a\right)^{\nu}$, where κ_a, T_a are the thermal conductivity and temperature calculated at the peak density, and ν is the power index. These simplifications make the problem solvable with analytic techniques.[8–12,14] If the radiated energy is negligible (low-Z materials, such as DT), the energy is transported mainly by electronic heat conduction. In this case, the power index $\nu = 2.5$ (as given by Spitzer[23]) and $L_0 = \left(\gamma_h - 1\right)/\gamma_h A \kappa_a / \left(\rho_a V_a\right)$, where γ_h is the ratio of the specific heats, $A = m_i/(1+Z)$ is the average particle mass, ρ_a is the maximum density, and V_a is the ablation velocity, respectively (see Ref. 8). However, if a significant amount of energy is present in the radiation field, then an accurate estimate of the energy transport requires the use of multigroup radiation transport models. In such models, the radiation energy spectrum is divided into several groups. Each group is described by a radiation temperature obeying an energy diffusion equation. Because of the complexity of such models, an analytic stability analysis would be intractable. For such reason, the analytic theories are based on a single-group model (one temperature). However, if the one-group diffusive transport model is used in the stability analysis, then one should at least make sure that such a model reproduces the one-dimensional hydrodynamic profiles obtained using the multigroup model. In other words, one should fit the multigroup hydro-profiles with the one-group profiles by properly selecting the value of ν and L_0. This is an essential requirement for the stability analysis, assuring that the linearization is performed about the right equilibrium. Of course, there is no guarantee that the two-dimensional effects are correctly included in the one-group model, even though the one-dimensional profiles are correctly reproduced. However, the RT is mainly a hydrodynamic instability, and one could hope that if the 1-D hydrodynamic profiles are correctly included, then the 2-D/3-D stability analysis would be independent of the heat transport model. This speculation could be verified *a posteriori* by comparing the analytic results with 2-D simulations including multigroup radiation transport.

In summary, the analytic analysis is based on the one-group subsonic diffusive transport model (or isobaric model). The parameters ν, Fr, and L_0 of such a model are determined by fitting the analytic hydro-profiles with those obtained from 1-D simulations including multigroup radiation transport. The results of the analytic stability theory are then compared with the full 2-D simulations including multigroup radiation transport.

As shown in Ref. 6, the density profile of subsonic ablation fronts, described by the one-temperature diffusive transport model, obeys the following first-order differential equation:

$$d\xi/dy = -\xi^{\nu+1}\left(1-\xi\right)/L_0 , \qquad (9)$$

where ξ is the density normalized to its peak value, $\xi = \rho/\rho_a$, and ν is the power index for thermal conduction. The equilibrium pressure is determined by the momentum-conservation equation $d\left(p+\rho U^2\right)/dy = \rho g$ and the mass conservation equation $\left[d\left(\rho U\right)/dy = 0\right]$, which can be rewritten in the following dimensionless form:

$$\frac{1}{\Pi_a}\frac{d\,\Pi}{dy} = \xi^2\frac{d\xi}{dy} + \frac{\xi}{Fr\,L_0}, \qquad \xi U(y) = V_a , \qquad (10)$$

where $\Pi = p/p_a$, $\Pi_a = V_a/\sqrt{p_a/\rho_a}$ is the normalized ablation velocity, and p_a is the pressure at the location of the peak density ρ_a. Observe that Eqs. (9) and (10) for the unknowns ξ and Π depend on the four parameters Π_a, Fr, L_0, and ν. Keeping in mind that our goal is to reproduce the hydro-profiles of the 1-D simulations, we determine these parameters by fitting the analytic hydro-profiles with the numerical ones. Let's define with $\xi_s = \rho/\rho_a$ and $\Pi_s = p/p_a$ the normalized simulated

density and pressure profiles. If the predictions of the one-group model were exact, then the simulated profiles would represent an exact solution of Eqs. (9) and (10); however, this is not the case, and replacing ξ with ξ_s in Eq. (9) leads to an error. For convenience, we take the logarithm of Eq. (9) and define the error as

$$\mathrm{er} = (\nu+1)\ln\xi_s - \ln L_0 - \ln\left(-\frac{d\xi_s}{dy}\,\frac{1}{1-\xi_s}\right). \quad (11)$$

Observe that er = 0 if $\xi_s = \xi$. In order to reproduce the simulated profiles over the entire ablation front, it is useful to minimize the integrated quadratic error (δ) defined as

$$\delta(\nu, L_0) \equiv \int_{\xi_{\min}}^{\xi_{\max}} \left[(\nu+1)\ln\xi_s - \ln L_0 - \ln\left(-\frac{d\xi_s}{dy}\,\frac{1}{1-\xi_s}\right)\right]^2 d\xi_s, \quad (12)$$

where $\xi_{\min}$, $\xi_{\max}$ are the minimum and the maximum values of the density of the fitting region defining the extension of the ablation front ($\xi_{\min} = 0.01$ and $\xi_{\max} = 0.99$ are two possible values). The minimization of δ is obtained by setting to zero the partial derivatives with respect to ν and L_0:

$$\frac{\partial\delta}{\partial L_0} = \frac{\partial\delta}{\partial\nu} = 0. \quad (13)$$

Substituting Eq. (12) into Eq. (13) leads to the following estimates of L_0 and ν:

$$\nu = \frac{c_1a_1 - c_2b_1}{a_1^2 - a_2b_1} - 1, \qquad L_0 = \exp\left(\frac{+a_2c_1 - a_1c_2}{a_1^2 - a_2b_1}\right), \quad (14)$$

where

$$a_1 = [\![\xi(\ln\xi - 1)]\!], \quad (15a)$$

$$a_2 = [\![\xi(\ln\xi - 1)^2 + \xi]\!], \quad b_1 = [\![\xi]\!],$$

$$c_1 = \int_{y(\xi_{\min})}^{y(\xi_{\max})} \ln\left[-\frac{d\xi_s}{dy}\,\frac{1}{1-\xi_s}\right]\frac{d\xi_s}{dy}\,dy, \quad (15b)$$

$$c_2 = \int_{y(\xi_{\min})}^{y(\xi_{\max})} \ln\xi_s \ln\left[-\frac{d\xi_s}{dy}\,\frac{1}{1-\xi_s}\right]\frac{d\xi_s}{dy}\,dy, \quad (15c)$$

and $[\![H(\xi)]\!] = H(\xi_{\max}) - H(\xi_{\min})$. In the same fashion, the Froude number and dimensionless ablation velocity Π_a can be determined by minimizing the integrated quadratic error η in the momentum conservation equation

$$\eta(Fr, \Pi_a) = \int_{y(\xi_{\min})}^{y(\xi_{\max})} \left(\frac{1}{\Pi_a^2}\,\frac{d\Pi_s}{dy} - \frac{1}{\xi_s^2}\,\frac{d\xi_s}{dy} - \frac{\xi_s}{FrL_0}\right)^2 dy, \quad (16)$$

where $\Pi_s = p_s/p_a$ is the simulated normalized pressure profile. After some straightforward algebra, the minimization with respect to Π_a and Fr yields

$$Fr = \frac{a_3b_4 + b_3^2}{b_3c_3 + a_3c_4}\,\frac{1}{L_0}, \qquad \Pi_a^2 = \frac{a_3b_4 + b_3^2}{c_3b_4 - c_4b_3}, \quad (17a)$$

where

$$a_3 = \int_{y(\xi_{\min})}^{y(\xi_{\max})} \left(\frac{d\Pi_s}{dy}\right)^2 dy, \quad (17b)$$

$$b_3 = -\int_{y(\xi_{\min})}^{y(\xi_{\max})} \xi_s\,\frac{d\Pi_s}{dy}\,dy,$$

$$b_4 = -\int_{y(\xi_{\min})}^{y(\xi_{\max})} \xi_s^2\,dy, \; c_3 = \int_{y(\xi_{\min})}^{y(\xi_{\max})} \frac{1}{\xi_s^2}\,\frac{d\Pi_s}{dy}\,\frac{d\xi_s}{dy}\,dy, \quad (17c)$$

$$c_4 = \ln\frac{\xi_{\max}}{\xi_{\min}}.$$

The integration limits $y(\xi_{\min})$, $y(\xi_{\max})$ represent the location of the points with density $\xi_{\min}$ and $\xi_{\max}$, respectively. Using the peak density ρ_a and the pressure at the location of the peak

density p_a, the acceleration and ablation velocity can be easily determined from Eqs. (14) and (17):

$$V_a = \Pi_a \sqrt{\frac{p_a}{\rho_a}}, \qquad g = \frac{V_a^2}{L_0}\,\frac{1}{Fr}. \tag{18}$$

This technique has been tested on the hydrodynamic profiles obtained using the code *LILAC*. We consider a planar CH foil of thickness $d = 18\ \mu$m irradiated by a 0.35-μm-wavelength laser of 50-TW/cm^2 intensity with a 1-ns linear ramp. The pulse duration is 3 ns. The profiles obtained from the simulation are slowly varying in time. For the test, we consider the profiles at time $t = 2$ ns and substitute the simulated density and pressure into Eqs. (14), (17), and (18) and obtain $\nu = 0.7$, $L_0 = 0.24\ \mu$m, $Fr = 0.032$, $g = 36\ \mu$m/ns^2, and $V_a = 0.54\ \mu$m/ns. Then, using these values, we solve Eqs. (9) and (10) to determine the analytic density and pressure profiles. Figure 73.27 shows the simulated and the analytic profiles for the CH target. The excellent agreement between the profiles shows the accuracy of the fitting procedure described above. In Fig. 73.28, the fitting parameters ν, L_0, and Fr are plotted as functions of time, and the dashed lines represent the corresponding average values. It is important to notice that the power index for thermal conduction to be used in the one-group model ($\nu = 0.7$) is well below the Spitzer[23] ($\nu = 2.5$) or the Zeldovich[24] value ($\nu \simeq 6.5$), thus showing the importance of the multigroup treatment of the radiation transport in plastic targets.

Lower-Z materials such as solid DT are a good test of the fitting procedure because they are expected to produce a very low level of radiation and to approximately follow the Spitzer model with $\nu \approx 2.5$. We have considered a planar DT foil of thickness $d = 120\ \mu$m irradiated by the pulse described above. Substituting the simulated profiles into Eqs. (9) and (10) yields $\nu = 2$, $L_0 = 0.03\ \mu$m, and $Fr = 5$. This result indicates that radiation transport has a small effect in cryogenic DT targets.

Tables 73.I and 73.II show the time-averaged values of Fr, ν, L_0, and V_a for several plastic (CH) and DT targets of different thicknesses (Th) and laser intensities (I). It is important to observe that plastic targets have smooth density profiles (large density-gradient scale length), low ablation velocity, $\nu < 1$, and small Froude numbers while solid-DT targets have sharp profiles, large ablation velocity, $\nu \approx 2$, and large Froude numbers.

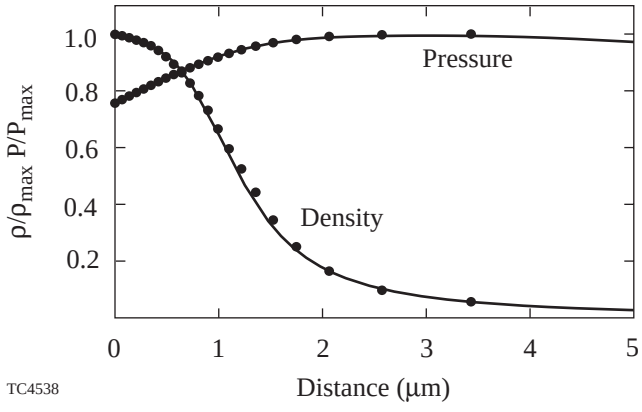

Figure 73.27
Normalized density and pressure profiles obtained by using isobaric model (solid lines) and 1-D numerical simulation (dots).

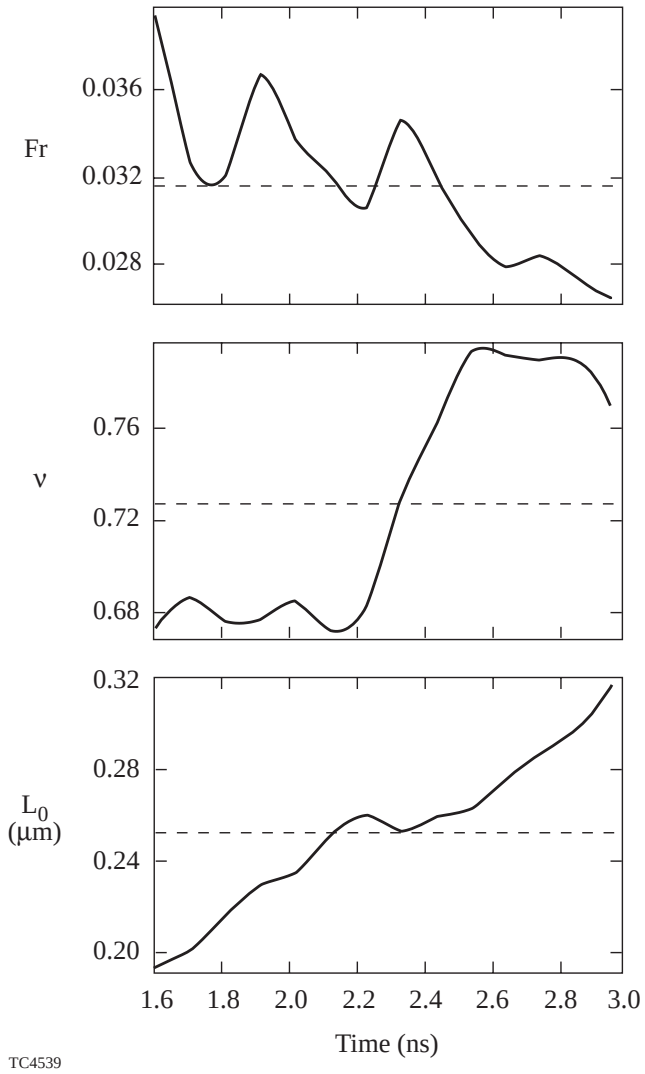

Figure 73.28
Temporal evolution (solid lines) and average values (dashed lines) of the Froude number Fr, power index for thermal conduction ν, and the characteristic thickness of ablation front L_0 for a CH target.

Growth Rates

1. Comparison with Numerical Results

Once the equilibrium parameters are calculated, Eq. (8) can be used to determine the growth rates. As discussed in the previous section, there is no guarantee that the analytic stability analysis using the one-temperature model would reproduce the results of the 2-D simulations using the multigroup radiation diffusion treatment even though the 1-D simulated and analytic hydrodynamic profiles are identical. It is necessary to validate the formula by comparing the analytic and the numerical growth rates.

As a first test of the analytic theory, we compare the analytic growth rates with Takabe's formula.[3] The latter has been derived by fitting the numerical solution of the exact, linearized, single-fluid conservation equations including Spitzer conductivity and a finite Mach number. This test is useful because it validates the assumption of subsonic flow and the simplification leading to the isobaric model.[5] Takabe's formula can be written in the following dimensionless form:[3]

$$\hat{\gamma} = \frac{\gamma}{\gamma_{\mathrm{cl}}} = \alpha_{\mathrm{T}} - \beta_{\mathrm{T}} X, \tag{19}$$

where $\gamma_{\mathrm{cl}} = \sqrt{kg}$ is the classical growth rate, $X = \sqrt{kV_a^2/g}$, $\alpha_{\mathrm{T}} \simeq 0.9$, and $\beta_{\mathrm{T}} \simeq 3.1$. Similarly, Eq. (8) can also be rewritten in dimensionless form:

$$\hat{\gamma} = \sqrt{\hat{A}_{\mathrm{T}} + \delta^2 \frac{X^6}{Fr^2} + \left(\omega^2 - \frac{1}{\xi_l}\right) X^2} - \delta \frac{X^3}{Fr} - \hat{\beta} X. \tag{20}$$

Table 73.I: CH targets.

Th (μm)	I (TW/cm^2)	$\langle Fr \rangle$	$\langle \nu \rangle$	$\langle L_0 \rangle$ (μm)	$\langle L_m \rangle$ (μm)	$\langle V_a \rangle$ (μm/ns)	$\langle g \rangle$ (μm/ns^2)	Growth Rate [fit of Eq. (8)]
10	50	0.03	0.8	0.2	0.7	0.8	95	$1.01\sqrt{\frac{kg}{1+kL_m}} - 1.8\,kV_a$
18	50	0.03	0.8	0.3	1.0	0.6	50	$1.01\sqrt{\frac{kg}{1+kL_m}} - 1.8\,kV_a$
20	100	0.04	0.9	0.3	1.1	0.9	76	$0.99\sqrt{\frac{kg}{1+kL_m}} - 1.7\,kV_a$
20	240*	0.05	0.9	0.2	0.7	1.3	130	$0.97\sqrt{\frac{kg}{1+kL_m}} - 1.6\,kV_a$
25	240*	0.05	0.9	0.2	0.7	1.2	123	$0.98\sqrt{\frac{kg}{1+kL_m}} - 1.6\,kV_a$

*Linear-rise laser pulse

Table 73.II: DT targets.

Th (μm)	I (TW/cm^2)	$\langle Fr \rangle$	$\langle \nu \rangle$	$\langle L_0 \rangle$ (μm)	$\langle L_m \rangle$ (μm)	$\langle V_a \rangle$ (μm/ns)	$\langle g \rangle$ (μm/ns^2)	Growth Rate [fit of Eq. (8)]
100	50	4.1	2.0	0.02	0.13	2.8	97	$0.94\sqrt{kg} - 2.6\,kV_a$
190	50	3.8	2.0	0.03	0.20	2.7	60	$0.94\sqrt{kg} - 2.6\,kV_a$
190	100	4.0	2.1	0.07	0.49	4.6	77	$0.94\sqrt{kg} - 2.6\,kV_a$

The growth rates calculated using Eq. (19) and Eq. (20) for ν = 2.5 and different Froude numbers are shown in Fig. 73.29. Observe that the two formulas approximately agree for Froude numbers between 0.1 and 5. This result is not surprising as Takabe's formula has been derived using Spitzer conductivity leading to sharp profiles (small L_0 and therefore relatively large Froude numbers). We conclude that the RT growth rate in low-Z materials with $Fr > 0.1$, such as solid DT, is well described by Takabe's formula over a wide range of Fr ($0.1 < Fr < 5$). For small Froude numbers or different values of ν, Takabe's formula doesn't provide an accurate estimate of the growth rate so Eq. (8) or its fitting formulas must be used.

When the ablation velocity is small or the density profile is smooth—as in the case of large radiation energy transport—we expect the Froude number to decrease. As shown in Fig. 73.29, Takabe's formula and Eq. (8) yield very different results for this case. In addition, radiative transport causes the deviation of the power index ν from the Spitzer value requiring a more general formula than Takabe's. For such targets, Eq. (8) can be compared only with the results of full 2-D simulations including a multigroup radiation-transport model. We consider the same 18-μm plastic target described in the previous section, and we simulate it with the code *ORCHID*. We then calculate the parameters ν, Fr, L_0, and V_a to be used in Eq. (8) by substituting *ORCHID* density and pressure profiles into Eqs. (14), (17), and (18) and find $Fr = 0.043$, $L_0 = 0.24$ μm, $V_a = 0.66$ μm/ns, $\nu = 0.96$, and $g = 43$ μm/ns^2. In Fig. 73.30, the growth rates obtained using *ORCHID* (dots) are compared with Eq. (8) (solid line), Takabe's (dot–dashed line), and modified Takabe's (dashed line) formulas. The latter is the Takabe's formula including the stabilizing effects of finite density-gradient scale length in a heuristic fashion,

$$\gamma_{\text{m.T.}} = \alpha_T \sqrt{\frac{kg}{1+kL_m}} - \beta_T k V_a , \qquad (21)$$

where L_m is the minimum density-gradient scale length, L_m = 0.93 μm. Observe that Takabe's and modified Takabe's formulas fail to reproduce the simulation results in the short-wavelength regime. Instead, the growth rates obtained with Eq. (8) are in excellent agreement with the simulated ones over the entire unstable spectrum.

Furthermore, we study different pulse shapes and different target materials. We consider a 20-μm-thick CH target irradiated by a square pulse with an intensity of 200 TW/cm^2 and 100-ps linear rise time. According to the *ORCHID* simulations, the hydrodynamic profiles reach a steady state after 1.3 ns. The growth rates of 30-μm and 15-μm wavelength perturbations are determined from the 2-D simulations yielding γ^{sim} (15 μm) = 4.9 ns^{-1} and γ^{sim} (30 μm) = 4.1 ns^{-1}. Using the *ORCHID* hydrodynamic profiles and Eqs. (14), (17), and (18), we estimate the relevant hydrodynamic parameters $\nu = 1.2$, L_0 = 0.22 μm, V_a = 2.0 μm/ns, Fr = 0.12, and g = 144 μm/ns^2. Substituting such parameters into the asymptotic formula [Eq. (8)] yields the theoretical growth rates γ^{th} (15 μm) = 4.9 ns^{-1} and γ^{th} (30 μm) = 4.06 ns^{-1}, reproducing the simulation results.

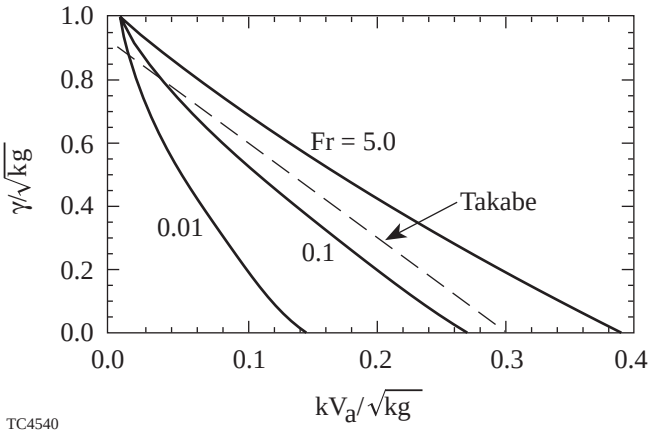

Figure 73.29
Normalized growth rate $\left(\gamma/\sqrt{kg}\right)$ versus normalized wave number $\left(\sqrt{kV_a^2/g}\right)$ calculated using the Takabe's formula (dashed line) and Eq. (8) (solid line) for different values of the Froude number and $\nu = 2.5$.

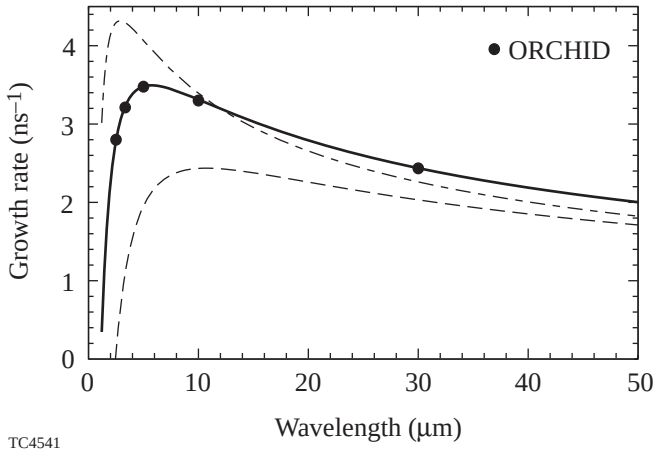

Figure 73.30
Unstable spectrum calculated using the analytic formula (8) (solid line) compared with the numerical results (dots) of 2-D hydrocode *ORCHID*, Takabe's formula (dot-dashed line) and modified Takabe's formula (dashed line).

Next, we simulate the evolution of 6-μm-wavelength surface perturbation on a 20-μm-thick beryllium foil irradiated by a square pulse with an intensity of 50 TW/cm^2 and 100-ps linear rise time. The steady state is reached after 1.5 ns and the *ORCHID* simulation yields the mode growth rate $\gamma^{\text{sim}} = 2.27\ \text{ns}^{-1}$. The simulated and analytic hydrodynamic profiles match for $\nu = 0.63$, $L_0 = 0.36\ \mu$m, $V_a = 0.73\ \mu$m/ns, $Fr = 0.06$, and $g = 25\ \mu\text{m/ns}^2$, thus yielding the theoretical growth rate $\gamma^{\text{th}} = 2.28\ \text{ns}^{-1}$ in good agreement with the numerical simulations.

These tests are a clear indication that Eq. (8) can be used to determine the RT growth rates for ablation fronts with large/small Froude numbers and short-/long-wavelength perturbations.

2. Fitting Formula for the Growth Rate

Although Eq. (8) provides an accurate estimate of the ablative RT growth rates, its expression is too complicated for practical applications. Without a doubt, a simplification of Eq. (8) would greatly help the target designers in the choice of the ablator material and the implementation of the RT mixing models. For this purpose, we simplify Eq. (8) using two well-known fitting formulas:

$$\gamma_1 = \alpha_1(Fr,\nu)\sqrt{kg} - \beta_1(Fr,\nu)kV_a, \qquad (22)$$

$$\gamma_2 = \alpha_2(Fr,\nu)\sqrt{\frac{kg}{1+kL_m}} - \beta_2(Fr,\nu)kV_a, \qquad (23)$$

where $L_m = L_0(\nu+1)^{\nu+1}/\nu^{\nu}$ is the minimum density-gradient scale length, and the α's and β's are functions of Fr and ν. It turns out that Eq. (22) is particularly accurate in fitting the large Froude number results, while Eq. (23) is suitable for low Froude numbers. This is not surprising as ablation fronts with small Froude numbers are unstable to modes with wavelengths smaller than the density-gradient scale length whose growth is strongly affected by the finite kL_m.

The calculation of the coefficients α_1, β_1 and α_2, β_2 is carried out using the standard fitting procedures of the Mathematica software package.[25] We define a range of interest for the mode wavelength from the cutoff λ_c to about 200 times the cutoff wavelength $\lambda_{\max} \approx 200\ \lambda_c$ (the parameters α and β have shown little sensitivity to the value of $\lambda_{\max}$). The α's and β's are determined by fitting the growth rate γ obtained using Eq. (8) with the formulas (22) and (23) over the wavelength range $\lambda_c < \lambda < \lambda_{\max}$. Figures 73.31 and 73.32 show the value of α, β for different Fr and ν. The solid section of the curves represents the region of optimum fit, i.e., the region where each formula fits the data at its best. According to the value of Fr and ν, one should use the formula corresponding to a solid curve.

As an example, we consider the plastic target used in the *ORCHID* simulations described in the previous section. The values $Fr = 0.043$ and $\nu = 0.96$ are obtained by processing the *ORCHID* hydro-profiles with the procedure described in the **Equilibrium Parameters** section. Using Fig. 73.32, we determine the optimum fit by using γ_2 with $\alpha_2 = 0.98$ and $\beta_2 = 1.64$. Figure 73.33 shows a plot of the unstable spectrum obtained using Eq. (8) (solid line) and the fitting formula γ_2 (dashed line). The excellent agreement between the two curves indicates that the fitting formula represents a good approximation of Eq. (8).

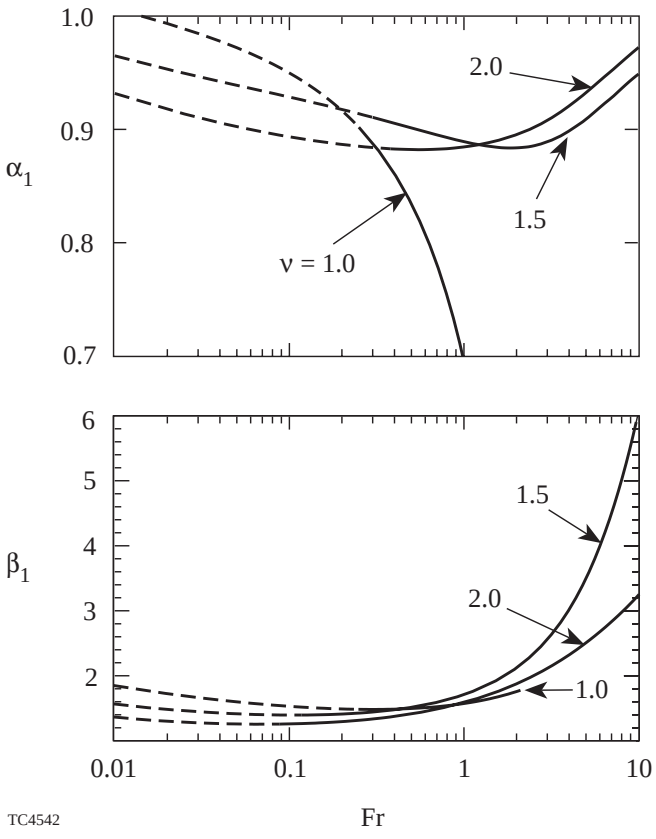

Figure 73.31
Plot of coefficients α_1, β_1 of the fitting formula (22) versus Froude number for different values of the power index ν. Solid line represents the regions of the best fit of the analytical formula (8) with Eq. (22).

We have determined the optimum fit for several plastic and solid-DT targets commonly used in direct-drive ICF experiments. Table 73.I shows the results of the fitting procedure described above for different laser pulses and plastic target thicknesses. It appears that over a wide range of thicknesses and laser powers, the growth rate of the RT instability for directly driven CH targets can be approximated by

$$\gamma_{\mathrm{CH}} \approx 0.98\sqrt{\frac{kg}{1+kL_m}} - 1.7\ kV_a\,, \tag{24}$$

where $0.6 < L_m < 1\ \mu$m. The same formula has been derived for the aluminum-coated CH and beryllium targets. The corresponding time-averaged values of Fr, ν, L_0, g, and V_a are shown in Tables 73.III and 73.IV, respectively. The growth rate for cryogenic DT targets is better represented by the fit γ_1, and Table 73.II shows the optimum fit for different flat targets driven by a 1-ns linear ramp followed by a flat-top pulse. These results indicate that the growth rate of solid-DT targets is well approximated by a Takabe-like formula

$$\gamma_{\mathrm{DT}} \approx 0.94\sqrt{kg} - 2.7\ kV_a\,. \tag{25}$$

The RT growth rate for different ablator materials can be determined in the same fashion by using 1-D hydro-simulations to reproduce the density and pressure profiles; Eqs. (14), (17), and (18) to calculate the equilibrium parameters; and Figs. 73.31 and 73.32 to generate the growth-rate formulas.

It is very important that the 1-D hydrodynamic analytic profiles be carefully matched with the simulation results when determining the relevant equilibrium parameters. Even though the analytic theory yields satisfactory results for DT, CH, and Be targets, it might fail to reproduce the profiles of other materials. For instance, the hydrodynamic profiles of plastic targets with high-Z dopants are not well reproduced by the single temperature model, and Eq. (8) cannot be applied to determine the RT growth rate. The study of the RT instability in such targets is currently under investigation.

An interesting result of the analytic theory concerns those equilibria with $\nu \simeq 1$ and $Fr > 2$. Figure 73.31 shows that α_1 decreases dramatically with increasing Froude numbers. This result is not surprising as the same conclusion can be reached using the results of the self-consistent stability analysis of Ref. 9 reported in Eq. (5). The growth-rate formula (5) yields zero growth rate for equilibria with $\nu = 1$ and $Fr > 2$ when the

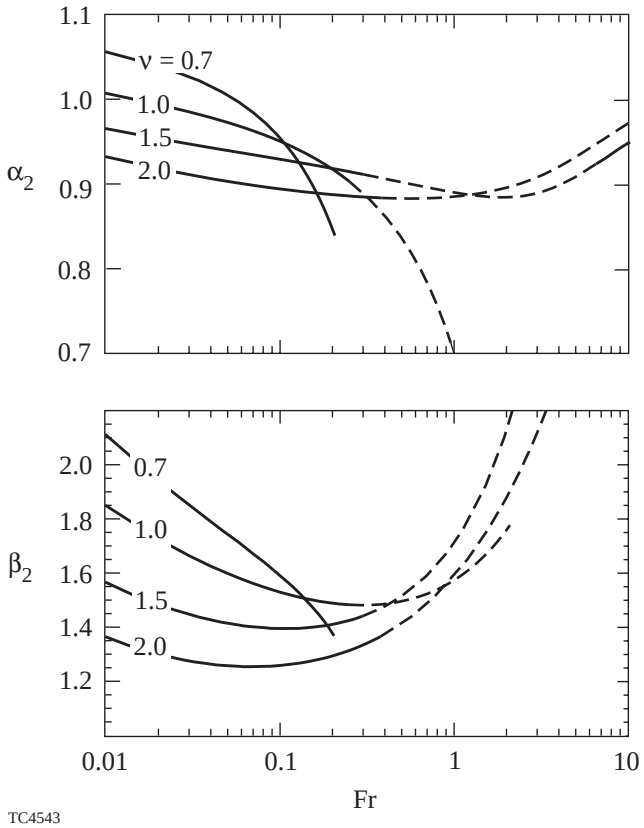

Figure 73.32
Plot of coefficients α_2, β_2 of the fitting formula (23) versus Froude number for different values of the power index ν. Solid line represents the regions of the best fit of the analytical formula (8) with Eq. (23).

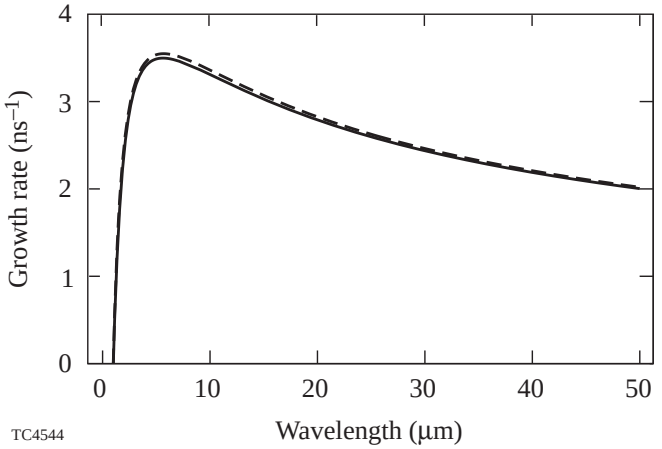

Figure 73.33
Unstable spectrum of the target described in the **Equilibrium Parameters** section calculated using the analytic formula (8) (solid line) and the fitting formula (23) (dashed line).

Table 73.III: Be targets.

Th (μm)	I (TW/cm^2)	$\langle Fr \rangle$	$\langle \nu \rangle$	$\langle L_0 \rangle$ (μm)	$\langle L_m \rangle$ (μm)	$\langle V_a \rangle$ (μm/ns)	$\langle g \rangle$ (μm/ns^2)	Growth Rate [fit of Eq. (8)]
16	50	0.05	0.7	0.2	0.6	0.6	40	$1.00\sqrt{\frac{kg}{1+k\,L_m}} - 1.7\ kV_a$
16	100	0.06	0.7	0.2	0.6	0.8	60	$0.99\sqrt{\frac{kg}{1+k\,L_m}} - 1.7\ kV_a$
32	100	0.06	0.6	0.4	1.2	0.8	28	$1.00\sqrt{\frac{kg}{1+k\,L_m}} - 1.7\ kV_a$
16	240*	0.10	0.8	0.1	0.4	1.1	28	$0.95\sqrt{\frac{kg}{1+k\,L_m}} - 1.7\ kV_a$

*Linear-rise laser pulse

Table 73.IV: CH targets with aluminum coating.

Th (μm)	I (TW/cm^2)	$\langle Fr \rangle$	$\langle \nu \rangle$	$\langle L_0 \rangle$ (μm)	$\langle L_m \rangle$ (μm)	$\langle V_a \rangle$ (μm/ns)	$\langle g \rangle$ (μm/ns^2)	Growth Rate [fit of Eq. (8)]
20+0.5	100	0.07	0.9	0.7	2.6	1.9	72	$0.97\sqrt{\frac{kg}{1+k\,L_m}} - 1.7\ kV_a$
20+1.0	100	0.08	0.7	1.6	5.0	2.8	63	$0.98\sqrt{\frac{kg}{1+k\,L_m}} - 1.7\ kV_a$

second term in the square root $-A_T^2 k^2 V_a V_{\text{b.o.}}$ (caused by overpressure of the blowoff region with respect to the overdense region) is larger than the instability-drive term $A_T kg$ for any wave number. This result has also been confirmed by solving the system (2)–(4) of Ref. 9 using an initial value code and is also in agreement with the numerical results of Kull (see Ref. 6). In addition, the numerical results seem to indicate that such a stabilization occurs for any $\nu \leq 1$. In conclusion, hydrodynamic profiles with $\nu \leq 1$ and $Fr > 2$ are RT stable for all wavelengths.

Conclusions

The growth rate of the ablative Rayleigh–Taylor instability is calculated using the analytic theory of Goncharov *et al*. (Ref. 11) and the output of one-dimensional simulations of laser-accelerated targets. The simulated density and pressure profiles are used to determine the equilibrium parameters Fr, V_a, g, ν, and L_0 via a newly developed fitting procedure. Those parameters are then substituted into the self-consistent growth-rate formula of Goncharov *et al*. (Ref. 11). The accuracy of such a procedure has been tested by comparing the analytic growth rates for a plastic target with the ones obtained using two-dimensional simulations. This theory suggests that Takabe's formula represents a good approximation of the growth rates for only relatively large Froude numbers ($0.1 < Fr < 5$) and electronic heat conduction ($\nu \simeq 2.5$) but fails for small Froude numbers and radiative materials. The complicated asymptotic formula of Ref. 11, which is valid for arbitrary Froude numbers, has been simplified by using simple fits over a wide range of Froude numbers and power indices for thermal conduction. In addition, simple growth-rate formulas for solid DT, plastic (CH), and beryllium targets have been derived. Even though the analytic theory yields satisfactory results for DT, CH, and Be targets, it might not be adequate for other materials such as chlorinated plastic. The hydrodynamic profiles of plastic targets with high-Z dopants are not well reproduced by the single temperature model and Eq. (8) cannot be applied to determine the RT growth rate.

ACKNOWLEDGMENT

This work was supported by the U.S. Department of Energy Office of Inertial Confinement Fusion under Cooperative Agreement No. DE-FC03-92SF19460, the University of Rochester, and the New York State Energy Research and Development Authority. The support of DOE does not constitute an endorsement by DOE of the views expressed in this article.

REFERENCES

1. S. E. Bodner, Phys. Rev. Lett. **33**, 761 (1974).
2. K. O. Mikaelian, Phys. Rev. A **42**, 4944 (1990).
3. H. Takabe *et al*., Phys. Fluids **28**, 3676 (1985).
4. C. P. Verdon, R. L. McCrory, R. L. Morse, G. R. Baker, D. I. Meiron, and S. A. Orszag, Phys. Fluids **25**, 1653 (1982).
5. H. J. Kull and S. I. Anisimov, Phys. Fluids **29**, 2067 (1986).
6. H. J. Kull, Phys. Fluids B **1**, 170 (1989).
7. J. D. Kilkenny, S. G. Glendinning, S. W. Haan, B. A. Hammel, J. D. Lindl, D. Munro, B. A. Remington, S. V. Weber, J. P. Knauer, and C. P. Verdon, Phys. Plasmas **1**, 1379 (1994).
8. R. Betti, V. N. Goncharov, R. L. McCrory, and C. P. Verdon, Phys. Plasmas **2**, 3844 (1995).
9. V. N. Goncharov, R. Betti, R. L. McCrory, P. Sorotokin, and C. P. Verdon, Phys. Plasmas **3**, 1402 (1996).
10. R. Betti, V. N. Goncharov, R. L. McCrory, P. Sorotokin, and C. P. Verdon, Phys. Plasmas **3**, 2122 (1996).
11. V. N. Goncharov, R. Betti, R. L. McCrory, and C. P. Verdon, Phys. Plasmas **3**, 4665 (1996).
12. A. R. Piriz, J. Sanz, and L. F. Ibanez, Phys. Plasmas **4**, 1117 (1997).
13. S. Atzeni, Nucl. Fusion **36**, 69 (1996).
14. J. Sanz, Phys. Rev. E **53**, 4026 (1996).
15. J. H. Nuckolls *et al*., Nature **239**, 139 (1972).
16. J. D. Lindl, Phys. Plasmas **2**, 3933 (1995).
17. Lord Rayleigh, in *Scientific Papers* (Cambridge University Press, Cambridge, England, 1900), Vol. II, pp. 200–207; G. Taylor, Proc. R. Soc. London Ser. A **201**, 192 (1950).
18. A. B. Bud'ko and M. A. Liberman, Phys. Fluids B **4**, 3499 (1992).
19. R. L. McCrory and C. P. Verdon, in *Computer Applications in Plasma Science and Engineering*, edited by A. T. Drobot (Springer-Verlag, New York, 1991).
20. J. Delettrez and E. B. Goldman, Laboratory for Laser Energetics Report No. 36, University of Rochester (1976).
21. J. T. Larsen and S. M. Lane, J. Quant. Spectrosc. Radiat. Transf. **51**, 179 (1994).
22. G. B. Zimmerman and W. L. Kruer, Comments Plasma Phys. Control. Fusion **2**, 51 (1975).
23. L. Spitzer, Jr. and R. Härm, Phys. Rev. **89**, 977 (1953).
24. Ya. B. Zel'dovich and Yu. P. Raizer, in *Physics of Shock Waves and High-Temperature Hydrodynamic Phenomena*, edited by W. D. Hayes and R. F. Probstein (Academic Press, New York, 1966), Vol. I, p. 152.
25. S. Wolfram, *The Mathematica Book*, 3rd ed. (Wolfram Media/ Cambridge University Press, 1996).